

# Establishing the Fundamental Magnetic Interactions in the Chiral Skyrmionic Mott Insulator $\text{Cu}_2\text{OSeO}_3$ by Terahertz Electron Spin Resonance

M. Ozerov,<sup>1,\*</sup> J. Romhányi,<sup>2,†</sup> M. Belesi,<sup>2</sup> H. Berger,<sup>3</sup> J.-Ph. Ansermet,<sup>3</sup> Jeroen van den Brink,<sup>2,4</sup>  
J. Wosnitzer,<sup>1,4</sup> S. A. Zvyagin,<sup>1</sup> and I. Rousochatzakis<sup>2,‡</sup>

<sup>1</sup>Dresden High Magnetic Field Laboratory (HLD), Helmholtz-Zentrum Dresden-Rossendorf, Dresden D-01328, Germany

<sup>2</sup>Leibniz Institute for Solid State and Materials Research, IFW, Dresden D-01069, Germany

<sup>3</sup>Institut de Physique de la Matière Condensée, Ecole Polytechnique Fédérale de Lausanne, Station 3, CH-1015 Lausanne-EPFL, Switzerland

<sup>4</sup>Department of Physics, TU Dresden, Dresden D-01062, Germany

(Received 28 April 2014; published 7 October 2014)

The recent discovery of Skyrmions in  $\text{Cu}_2\text{OSeO}_3$  has established a new platform to create and manipulate Skyrmionic spin textures. We use high-field electron spin resonance with a terahertz free-electron laser and pulsed magnetic fields up to 64 T to probe and quantify its microscopic spin-spin interactions. In addition to the previously observed long-wavelength Goldstone mode, this technique probes also the high-energy part of the excitation spectrum which is inaccessible by standard low-frequency electron spin resonance. Fitting the behavior of the observed modes in magnetic field to a theoretical framework establishes experimentally that the fundamental magnetic building blocks of this Skyrmionic magnet are rigid, highly entangled and weakly coupled tetrahedra.

DOI: 10.1103/PhysRevLett.113.157205

PACS numbers: 75.40.Gb, 75.10.Jm, 76.30.-v

In recent years, there has been an enormous experimental activity in noncentrosymmetric helimagnets [1–8], where the chiral Dzyaloshinsky-Moriya (DM) interactions [9] stabilize Skyrmions, topological particlelike magnetization textures, originally introduced by Skyrme in the context of subatomic particle physics [10]. As first predicted by Bogdanov and Yablonskii [11], Skyrmions may condense spontaneously into a lattice at thermodynamic equilibrium [12], in analogy to Abrikosov vortices in type-II superconductors [13] or the “blue phases” in cholesteric liquid crystals [14]. While most of the well-known Skyrmionic helimagnets, such as MnSi [1,2],  $\text{Fe}_{1-x}\text{Co}_x\text{Si}$  [3,4], and FeGe [5] are metallic, the recent discovery [6–8] of Skyrmionic mesophases in  $\text{Cu}_2\text{OSeO}_3$ , a strongly correlated insulator with localized  $\text{Cu}^{2+}$  spins [15–17], has opened a route to explore Skyrmion physics in Mott insulators. In addition  $\text{Cu}_2\text{OSeO}_3$  manifests a magnetoelectric coupling [6,18,19] which brings exciting perspectives on the application front, since it allows us to manipulate Skyrmions by an external electric field [20–22].

Another very attractive aspect rooted in the insulating nature of  $\text{Cu}_2\text{OSeO}_3$  is that a reliable modeling of its magnetic interactions becomes possible which, in conjunction with powerful experimental techniques like the one presented below, offers the unique opportunity to gain a precise understanding of the microscopic magnetic structures and interactions in this Skyrmionic material. Having a noncentrosymmetric space group  $P2_13$ , the magnetic  $\text{Cu}^{2+}$  ions in  $\text{Cu}_2\text{OSeO}_3$  reside at the vertices of a distorted pyrochlore lattice, featuring two symmetry-inequivalent Cu sites, Cu1 and Cu2, with ratio 1:3 (in total, there are

16 Cu sites per unit cell); see Fig. 1. While the basic local magnetism is believed to be roughly pictured in terms of a semiclassical 3up-1down structure [15–17], density-functional-based band-structure calculations suggest that the basic building blocks of helimagnetism are not individual Cu spins but rather quantum-mechanical tetrahedral spin entities (shaded circle in Fig. 1) persisting far above the magnetic ordering temperature of  $T_C \approx 60$  K [23]. From the calculations, two well-separated exchange energy scales can be distinguished, defined by inter- and intratetrahedra exchange coupling interactions (hereafter, “weak” and “strong” interactions,  $|J_w| \sim 20\text{--}50$  K and

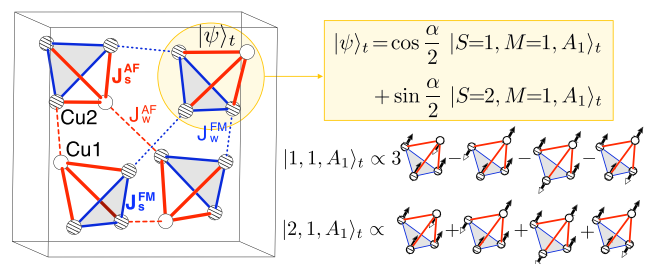


FIG. 1 (color online). Distorted pyrochlore structure of the  $\text{Cu}^{2+}$  ions in  $\text{Cu}_2\text{OSeO}_3$ , showing the proposed alternation of magnetically weak and strong tetrahedra. In total, there are five exchange couplings [23,25]: two strong,  $J_s^{\text{AF}}$  and  $J_s^{\text{FM}}$  (solid lines), two weak, connecting strong tetrahedra,  $J_w^{\text{AF}}$  and  $J_w^{\text{FM}}$  (dashed lines), and a weak longer-range exchange  $J_{\text{O-O}}^{\text{AF}}$  (not shown). The shaded circle indicates a strong tetrahedron with wave function  $|\psi\rangle_t$ , which strongly deviates from a semiclassical “3up-1down” state.

$|J_s| \sim 100\text{--}150$  K, respectively, Fig. 1). The rigid  $\text{Cu}_4$  entities are then engendered by the strong couplings  $J_s$ : the magnetic ground state (GS) of an isolated strong tetrahedron is separated from its excited states by a large gap of  $\Delta \approx 280$  K. Such a separation of energy scales identified by the calculations will very strongly affect the long-wavelength physics, the stability and interplay of Skyrmionic and half-Skyrmionic phases, the diameter of the Skyrmions, and the sign of the magnetic handedness, as well as the magnetoelectricity [23,24]. Here, we set out to prove its presence experimentally.

A direct fingerprint of the presence of weak and strong magnetic interactions will be in the magnetic excitation spectrum. In particular, weak interactions between tetrahedra, which do not alter the integrity of the strongly coupled tetrahedral entities, will cause a Goldstone mode plus a threefold mode with energy  $E \propto J_w$  [24]. The strong interactions, in turn, will cause the presence of a large number (56) of single-particle modes which correspond to local, intratetrahedra excitations that appear at higher energies ( $E \propto J_s$ ). Probing this magnetic mode structure requires not only access to a wide frequency range reaching up to the far infrared but also the ability for fine-tuning through a forest of strong phonon absorption lines that are present in the same region [26,27]. Here, we achieve this goal by employing a high-field electron spin resonance (ESR) spectroscopy using pulsed magnetic fields up to 64 T and a terahertz (THz) free-electron laser as a high-power monochromatic source in the range 1.2–70 THz. As we show below, this powerful technique gives direct access not only to the long-wavelength Goldstone mode, which has also been accessed by low-frequency (GHz-range) ESR [19,28,29] but also to the high-energy part of the excitation spectrum. We will show that fitting these ESR lines to the

theoretical framework not only provides direct experimental evidence of the tetrahedral picture of  $\text{Cu}_2\text{OSeO}_3$ , but also unambiguously quantifies the microscopic exchange couplings. This is especially important for the set of strong coupling parameters  $J_s$  which cannot be readily extracted from thermodynamic and magnetization measurements due to the large gap  $\Delta$  [30].

A high-quality single crystal of  $\text{Cu}_2\text{OSeO}_3$  was grown by chemical-vapor transport method. Experiments were performed on a  $2 \times 3 \times 1.42$  mm<sup>3</sup> piece using a pulsed-field ESR spectrometer and a THz-range free-electron laser at the Helmholtz-Zentrum Dresden-Rossendorf [31,32]. The latter employs a superconducting linear accelerator with pulse repetition rate of 13 MHz. This provides an operation of the THz laser in a quasi-cw mode with the radiation bandwidth of  $\sim 0.3\%$ – $0.7\%$  and intensity fluctuation less than 5%. This unique facility allows for ESR studies in the wavelength range of 4–250  $\mu\text{m}$  (which corresponds to 75–1.2 THz or wave number between 2500 and 40  $\text{cm}^{-1}$ ) and in pulsed magnetic fields up to 64 T and beyond [32]. VDI diodes (product of Virginia Diodes Inc.) were employed as radiation sources at frequencies below 0.5 THz. The base temperature of the sample was  $\sim 6$  K; that is well below the ordering temperature  $T_C$ . The magnetic field was applied along the cubic [001] crystallographic axis. We remark here that the magnitude of the applied field is always above the critical field  $H_{c2} \sim 0.1$  T where the transverse helical component triggered by the DM anisotropy vanishes [6,7,18].

The main experimental findings are shown on the frequency-magnetic field diagram in Fig. 2(a). The shading denotes the regions that suffer from low signal intensity due to strong phonon absorptions [Fig. 2(b)]. Four ESR modes,  $G$ ,  $A$ ,  $B$ , and  $C$  were detected in the frequency range

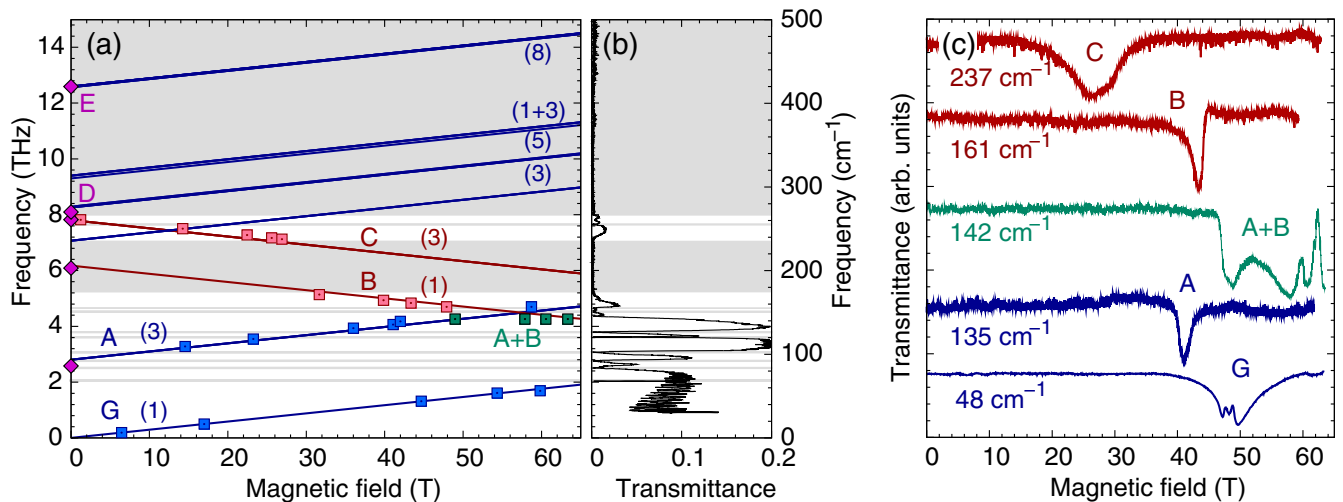


FIG. 2 (color online). (a) ESR spectral data for field along [100] and  $T \approx 6$  K. Lines are calculations (numbers give the degeneracy of each mode); see Fig. 3(c). Diamonds denote the absorption data reported by Raman [26] and far-infrared [27] studies; see text. Shaded areas show the regions with very low signal intensity due to strong phonon absorptions [27], as shown by the zero-field transmittance data at 4.2 K (b). (c) Examples of ESR spectra (the spectra are offset for clarity).

between 44 and 270  $\text{cm}^{-1}$ . In all cases, the relative ESR absorption was up to 60% compared to that in zero field. All the modes can be described using the effective  $g_{\text{eff}} \sim 2.1 \pm 0.1$ , typical for Cu ions. Extrapolating the frequency-field dependence of mode *B* to zero frequency gives the field  $H \approx 215$  T, where the minority Cu1 spins are flipped. Extrapolating the frequency-field dependences of modes *A*, *B*, and *C* to zero field, on the other hand, gives the zero-field gaps of 95, 202, and 263  $\text{cm}^{-1}$ , respectively. The mode *G* corresponds to the expected Goldstone mode that has also been seen in low-frequency studies [19,28,29,33].

Now, we would like to notice a fine structure of the resonance absorption observed at 142  $\text{cm}^{-1}$  in magnetic fields  $\sim 50$ –60 T [Fig. 2(c)]. This fine structure (which extends slightly above 60 T) corresponds to the level crossing of modes *A* and *B* and is consistent with the theoretical prediction that mode *A* is threefold degenerate (see below). Another important observation is that mode *C* (at a frequency of 237  $\text{cm}^{-1}$ ) is much broader than other modes, having a shoulder. This broadening is not related to thermal effects since (i) the temperature of the experiment (5–6 K) is one order of magnitude lower than  $T_C$ , and (ii) the lower-energy lines *A* and *B* are almost twice narrower. So the peculiar line shape of mode *C* reveals an internal structure, which is consistent with the theoretical prediction that this mode is also threefold degenerate (see below).

It is interesting to compare the ESR observations to the results from Raman scattering. Gnezdilov *et al.* [26] have reported a large number of modes; some of them can be regarded as magnetic excitations. These modes are shown in Figs. 2(a) and 3(c) by diamonds. The gaps of modes *B* and *C* (203 and 261  $\text{cm}^{-1}$ ) perfectly coincide with our observations, giving unambiguous evidence for their magnetic origin [34]. The modes *D* (270  $\text{cm}^{-1}$ ) and *E* (420  $\text{cm}^{-1}$ ) are exchange modes [Figs. 2(a) and 3(c)]. It is worth mentioning that lines *B* and *D* have also been reported in the far-infrared study of Miller *et al.* [27].

The theoretical treatment of the system with rigid tetrahedral entities that are weakly coupled can be achieved by expanding around a reference variational wave function  $|\Psi\rangle = \prod_i |\psi\rangle_i$ , which is the tensor product over the tetrahedral entities  $|\psi\rangle_i$ ; see Fig. 1 [24]. The latter can be found self-consistently by diagonalizing the mean-field Hamiltonian  $\mathcal{H}_{\text{TMF}}^{(t)} = \mathcal{H}_0^{(t)} + \mathcal{V}_{\text{MF}}^{(t)}$ , where  $\mathcal{H}_0^{(t)}$  contains the strong couplings  $J_s$  inside the tetrahedron  $t$ , and  $\mathcal{V}_{\text{MF}}^{(t)}$  contains the self-consistent mean fields exerted by neighboring tetrahedra  $t'$  on  $t$ , via the weak couplings  $J_w$ ; the explicit form of these Hamiltonians can be found in [35]. The remaining interactions described by  $\mathcal{H} - \sum_t \mathcal{H}_{\text{TMF}}^{(t)}$  can then be treated using a multiboson generalization of the standard spin-wave expansion. The main effect of these interactions is to weakly renormalize the energies and give

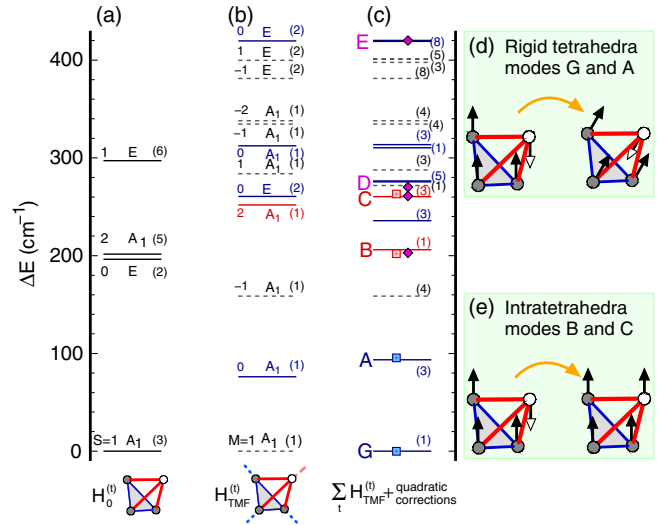


FIG. 3 (color online). (a) Spectrum of an isolated strong tetrahedron  $t$ ,  $H_0^{(t)}$  labeled by the IRs of  $C_{3v}$ , the total spin  $S$  of  $t$ , and its projection  $M$  along the  $z$  axis. (b) Spectrum of  $\mathcal{H}_{\text{TMF}}^{(t)} = \mathcal{H}_0^{(t)} + \mathcal{V}_{\text{MF}}^{(t)}$ , where  $\mathcal{V}_{\text{MF}}^{(t)}$  includes the exchange fields exerted by neighboring tetrahedra at a mean-field level. Here,  $S$  is not a good quantum number. (c) Zero-momentum excitations of the full Hamiltonian from quadratic multiboson theory. Solid lines denote states with  $M = 0$  or 2, that are accessible by ESR. (d),(e) Semiclassical pictures for two representative modes of different types.

rise to a finite dispersion. The correction to the GS expectation values of the local spin lengths is about 1% or less [24], showing that the GS correlations are captured almost entirely by the tetrahedra-factorized wave function  $|\Psi\rangle$  and that the method is internally consistent.

The resulting spectra of  $\mathcal{H}_0^{(t)}$  and  $\mathcal{H}_{\text{TMF}}^{(t)}$  for an isolated tetrahedron, as well as the final multiboson spectrum of the full Hamiltonian in the zero-momentum sector are shown, respectively, in Figs. 3(a), 3(b), and 3(c). Here the exchange couplings have been fitted to the experimental data (see details below). From the symmetries of the calculated wave functions, we can extract in detail the nature of the different magnetic modes. The spectrum of  $\mathcal{H}_0^{(t)}$  is classified in terms of the total spin  $S$  of the tetrahedron, its projection  $M$  along the  $z$  axis, as well as the irreducible representations (IRs) of the point group  $C_{3v}$ . The GS is a symmetric ( $A_1$ ) triplet followed by a pair of singlets belonging to the two-dimensional sector *E*, an  $A_1$  quintet, and, finally, a pair of triplets belonging to *E* [35]. Turning on the weak couplings  $J_w$  at the mean-field level does not lower the point group, and the total  $M$  remains a good quantum number, but this is not the case for the total spin  $S$ . As a result, the Zeeman degeneracy is lifted, and, in addition, we have a direct coupling between levels belonging to the same  $M$  and the same IR of  $C_{3v}$ . Most notably, the three components of the GS triplet  $\mathcal{H}_0^{(t)}$  split, and, in addition,

they admix a finite portion of the corresponding components of the  $A_1$  quintet; see formula for  $|\psi\rangle_t$  in Fig. 1. The remaining levels are affected analogously; see Fig. 3(b).

We are now ready to analyze the full excitation spectrum of Fig. 3(c), building on the main features of the spectrum of  $\mathcal{H}_{\text{TMF}}^{(t)}$  and by keeping in mind that there are four tetrahedra per unit cell. For concreteness, we shall only focus on the four lowest modes  $G$ ,  $A$ ,  $B$ , and  $C$  that are observed in our ESR experiments. These modes are dipolar; i.e., they correspond to transitions from  $|\psi\rangle_t$ , where  $M = 1$ , to states with  $M' = 0$  or  $2$ . Labeling the eigenstates of  $\mathcal{H}_{\text{TMF}}^{(t)}$  by an index  $n = 1-16$ , with  $n = 1$  corresponding to  $|\psi\rangle_t$ , there is one excitation per tetrahedron from  $n = 1$  to  $n' = 2$ , which in total gives four excitations with  $\delta M = M' - M = -1$ . The Goldstone mode  $G$  corresponds to the uniform combination, while the remaining three modes give the mode  $A$ , which belongs to the three-dimensional sector T of the space group  $P2_13$  of the wave vector  $\mathbf{k} = 0$ . Physically, the finite energy of this mode amounts to the energy cost of rotating one of the four tetrahedral entities against the mean field exerted by its neighbors. Importantly, the physical content of the rotated tetrahedron is not altered since the state  $|n' = 2\rangle \propto S^-|\psi_t\rangle$ ; i.e., it is simply a global rotation of  $|\psi\rangle_t$ .

The origin of modes  $B$  and  $C$  is fundamentally different, as they correspond to the four possible ways to excite from  $n = 1$  to  $n' = 6$ , which is a state that originates from the fully polarized (quintet) state of  $\mathcal{H}_0^{(t)}$ . In other words, this mode corresponds (semiclassically) to rotating the minority spin inside a single tetrahedron, which costs an energy  $E = 2J_s^{\text{AF}}$  at the level of  $\mathcal{H}_0^{(t)}$ . Again, there are four such modes per unit cell which, under the full space group of the  $\Gamma$  point, split into a onefold ( $A_1$ ) and a threefold (T) mode, corresponding, respectively, to modes  $B$  and  $C$ . In contrast to modes  $G$  and  $A$  which have  $\delta M = -1$  and, thus, become harder in a magnetic field,  $B$  and  $C$  have  $\delta M = +1$  and, thus, become softer in a field. Incidentally,  $B$  is the first mode that condenses at larger fields, marking the transition to the fully polarized state, as mentioned above. We also note in passing that the modes  $A$  and  $C$  do not belong to the symmetric representation  $A_1$  of  $P2_13$ , and so their detection by ESR is possible only due to anisotropy and the symmetry inequivalence of the electronic  $g$  tensors of the two Cu sites.

In addition to clarifying the nature of the observed modes, their multiplicity, and their behavior under a magnetic field, we also obtain direct information on the exchange couplings. As a guiding principle, we keep the weak-coupling values of Ref. [23] intact (namely,  $J_w^{\text{AF}} = 27$  K,  $J_w^{\text{FM}} = -50$  K, and  $J_{\text{O.O}}^{\text{AF}} = 45$  K). Since these couplings directly determine the system's thermodynamic properties, they can be considered fixed by fits to the experimental magnetization data [23]. In fact, the striking agreement in the energy of our ESR mode  $A$ , which

depends practically only on  $J_w$ , gives a direct experimental verification of these values. The strong coupling  $J_s^{\text{AF}}$  can be extracted from the energies of modes  $B$  and  $C$ , which depend only on this parameter [35], giving us  $J_s^{\text{AF}} \approx 145$  K. The second strong coupling  $J_s^{\text{FM}}$  can be extracted by fitting the mode  $E$  (observed by Raman scattering [26]) to the highest excitation originating from the twofold triplet state of Fig. 3(a), which fixes  $J_s^{\text{FM}} \approx -140$  K. These values are comparable to the calculated ones of 170 and  $-128$  K [23], be it 10%–15% lower.

In summary, we have performed a high-field resonance study of the chiral helimagnet  $\text{Cu}_2\text{OSeO}_3$  using pulsed magnetic fields up to 64 T and a terahertz-range free-electron laser as a high-power monochromatic source, enabling fine-tuning over a broadband frequency range and through a forest of strong phonon absorption regions. Apart from detecting the long-wavelength Goldstone excitation, several higher energy modes are disclosed. Comparing these results to a theoretical framework clarifies the detailed nature of the observed modes and allows us to unambiguously extract the magnetic interaction parameters. These findings establish experimentally that the fundamental magnetic building blocks of  $\text{Cu}_2\text{OSeO}_3$  are rigid, highly entangled tetrahedra, on account of a large separation of exchange energy scales. The latter has been shown to dramatically affect the long-wavelength helimagnetism, the presence of antiferromagnetic canting modes, the interplay of Skyrmionic and half-Skyrmionic phases [23], as well as the magnetoelectricity [24].

We thank W. Seidel for his help in preparing and operating free-electron laser. We acknowledge the support of the HLD-HZDR, member of the European Magnetic Field Laboratory (EMFL). S. A. Z. appreciates the support of the DFG.

---

\*Corresponding author.

m.ozarov@hzdr.de

†Corresponding author.

j.romhanyi@ifw-dresden.de

‡Corresponding author.

i.rousoschatzakis@ifw-dresden.de

- [1] S. Mühlbauer, B. Binz, F. Jonietz, C. Pfleiderer, A. Rosch, A. Neubauer, R. Georgii, and P. Böni, *Science* **323**, 915 (2009).
- [2] A. Tonomura, X. Yu, K. Yanagisawa, T. Matsuda, Y. Onose, N. Kanazawa, H. S. Park, and Y. Tokura, *Nano Lett.* **12**, 1673 (2012).
- [3] X. Z. Yu, Y. Onose, N. Kanazawa, J. H. Park, J. H. Han, Y. Matsui, N. Nagaosa, and Y. Tokura, *Nature (London)* **465**, 901 (2010).
- [4] W. Münzer, A. Neubauer, T. Adams, S. Mühlbauer, C. Franz, F. Jonietz, R. Georgii, P. Böni, B. Pedersen, M. Schmidt, A. Rosch, and C. Pfleiderer, *Phys. Rev. B* **81**, 041203 (2010).

- [5] X. Yu, N. Kanazawa, W. Zhang, T. Nagai, T. Hara, K. Kimoto, Y. Matsui, Y. Onose, and Y. Tokura, *Nat. Commun.* **3**, 988 (2012).
- [6] S. Seki, X. Z. Yu, S. Ishiwata, and Y. Tokura, *Science* **336**, 198 (2012).
- [7] T. Adams, A. Chacon, M. Wagner, A. Bauer, G. Brandl, B. Pedersen, H. Berger, P. Lemmens, and C. Pfleiderer, *Phys. Rev. Lett.* **108**, 237204 (2012).
- [8] S. Seki, J.-H. Kim, D. S. Inosov, R. Georgii, B. Keimer, S. Ishiwata, and Y. Tokura, *Phys. Rev. B* **85**, 220406 (2012).
- [9] I. Dzyaloshinsky, *J. Phys. Chem. Solids* **4**, 241 (1958); T. Moriya, *Phys. Rev. Lett.* **4**, 228 (1960).
- [10] T. Skyrme, *Nucl. Phys.* **31**, 556 (1962).
- [11] A. N. Bogdanov and D. A. Yablonskii, *Sov. Phys. JETP* **68**, 101 (1989); **69**, 142 (1989).
- [12] U. K. Rößler, A. N. Bogdanov, and C. Pfleiderer, *Nature (London)* **442**, 797 (2006).
- [13] A. A. Abrikosov, *Sov. Phys. JETP* **5**, 1174 (1957).
- [14] D. C. Wright and N. D. Mermin, *Rev. Mod. Phys.* **61**, 385 (1989).
- [15] K. Kohn, *J. Phys. Soc. Jpn.* **42**, 2065 (1977).
- [16] J.-W. G. Bos, C. V. Colin, and T. T. M. Palstra, *Phys. Rev. B* **78**, 094416 (2008).
- [17] M. Belesi, I. Rousochatzakis, H. C. Wu, H. Berger, I. V. Shvets, F. Mila, and J. P. Ansermet, *Phys. Rev. B* **82**, 094422 (2010).
- [18] M. Belesi, I. Rousochatzakis, M. Abid, U. K. Rößler, H. Berger, and J.-P. Ansermet, *Phys. Rev. B* **85**, 224413 (2012).
- [19] A. Maisuradze, A. Shengelaya, H. Berger, D. M. Djokić, and H. Keller, *Phys. Rev. Lett.* **108**, 247211 (2012).
- [20] J. S. White, I. Levatic, A. A. Omrani, N. Egetenmeyer, K. Prsa, I. Zivkovic, J. L. Gavilano, J. Kohlbrecher, M. Bartkowiak, H. Berger, and H. M. Ronnow, *J. Phys. Condens. Matter* **24**, 432201 (2012).
- [21] S.-Z. Lin, C. Reichhardt, C. D. Batista, and A. Saxena, *Phys. Rev. Lett.* **110**, 207202 (2013).
- [22] A. Fert, V. Cros, and J. Sampaio, *Nat. Nanotechnol.* **8**, 152 (2013).
- [23] O. Janson, I. Rousochatzakis, A. A. Tsirlin, M. Belesi, A. A. Leonov, U. K. Rößler, J. van den Brink, and H. Rosner, *arXiv:1403.2921* [*Nat. Commun. (to be published)*].
- [24] J. Romhányi, J. van den Brink, and I. Rousochatzakis, *arXiv:1403.4081*.
- [25] J. H. Yang, Z. L. Li, X. Z. Lu, M.-H. Whangbo, S.-H. Wei, X. G. Gong, and H. J. Xiang, *Phys. Rev. Lett.* **109**, 107203 (2012).
- [26] V. P. Gnezdilov, K. V. Lamonova, Y. G. Pashkevich, P. Lemmens, H. Berger, F. Bussy, and S. L. Gnatchenko, *Low Temp. Phys.* **36**, 550 (2010).
- [27] K. H. Miller, X. S. Xu, H. Berger, E. S. Knowles, D. J. Arenas, M. W. Meisel, and D. B. Tanner, *Phys. Rev. B* **82**, 144107 (2010).
- [28] A. Larrañaga, J. L. Mesa, L. Lezama, J. L. Pizarro, M. I. Arriortua, and T. Rojo, *Mater. Res. Bull.* **44**, 1 (2009).
- [29] M. I. Kobets, K. G. Dergachev, E. N. Khatsko, A. I. Rykova, P. Lemmens, D. Wulferding, and H. Berger, *Low Temp. Phys.* **36**, 176 (2010).
- [30] For example, the value of  $T_C$  is almost entirely fixed by the weak couplings  $J_w$  alone [23].
- [31] M. Ozerov, Ph.D. thesis, TU Dresden, 2011, <http://nbn-resolving.de/urn:nbn:de:bsz:14-qucosa-69892>.
- [32] S. A. Zvyagin, M. Ozerov, E. Cizmár, D. Kamenskyi, S. Zherlitsyn, T. Herrmannsdörfer, J. Wosnitza, R. Wünsch, and W. Seidel, *Rev. Sci. Instrum.* **80**, 073102 (2009).
- [33] In reality, the Goldstone mode is gapped (in zero field) due to magnetic anisotropy. The low-field ESR study by Kobets *et al.* [29] reports a spin-gap of about 3 GHz ( $\sim 0.1$  T), which is consistent with the energy scale of  $H_{c2}$ , itself mainly set by the DM anisotropy [6,7,18,23].
- [34] We note that the mode at  $86\text{ cm}^{-1}$ , observed by means of Raman scattering [26], was interpreted as the collective vibration of the edge-sharing  $\text{CuO}_5$  units [27].
- [35] See Supplemental Material at <http://link.aps.org/supplemental/10.1103/PhysRevLett.113.157205> for the eigenspectra of  $\mathcal{H}_0^{(r)}$  and  $\mathcal{H}_{\text{TMF}}^{(r)}$  and a detailed analysis of the influence of the various exchange couplings on the final excitation spectrum.